Unraveling anomalous isotope effect on hydrogen diffusivities in fcc metals from first principles including nuclear quantum effects

Hajime Kimizuka,[1,*] Shigenobu Ogata,[1,2] and Motoyuki Shiga[3]

[1]*Department of Mechanical Science and Bioengineering, Osaka University, Osaka 560-8531, Japan*

[2]*Center for Elements Strategy Initiative for Structural Materials, Kyoto University, Kyoto 606-8501, Japan*

[3]*Center for Computational Science and E-Systems, Japan Atomic Energy Agency, Chiba 277-0871, Japan*

(Received 9 September 2018; revised manuscript received 20 June 2019; published 8 July 2019)

The behavior of H isotopes in crystals is a fundamental and recurrent theme in materials physics. Especially, the information on H diffusion over a wide temperature range provides a critical insight into the quantum mechanical nature of the subject; however, this is not yet fully explored. From state-of-the-art *ab initio* calculations to treat both electrons and nuclei quantum mechanically, we found that the temperature dependence of H isotope diffusivities in face-centered-cubic (fcc) Pd has an unconventional "reversed S" shape on Arrhenius plots. Such irregular behavior is ascribed to the competition between different nuclear quantum effects with different temperature and mass dependencies, which leads to a peculiar situation, where the heavier tritium (^{3}H) diffuses faster than the lighter protium (^{1}H) in the limited temperature range of 80–400 K. This unveils the mechanism of anomalous crossovers between the normal and reversed isotope effects observed in the experiments at high and low temperatures.

DOI: 10.1103/PhysRevB.100.024104

I. INTRODUCTION

The behavior of H and its isotopes through materials has received significant attention, insofar as its understanding is crucial to developing technological applications with H as an energy source or carrier. These applications include H storage and purification, electrolyte and electrode materials for use in batteries and fuel cells, and nuclear fusion reactor technology [1–4]. However, owing to technical difficulties involved in measuring the lattice diffusion coefficient (D) accurately, even for very common metals, the D data measured by different techniques are fragmented and unevenly distributed over a wide temperature range [5,6]. In general, the nuclear quantum effects (NQEs) [7,8] of lightweight H, which include zero-point motion, discrete vibrational levels, and tunneling, are essential for characterizing the inherent picture and precise kinetics of H diffusion. In the case of face-centered-cubic (fcc) metals, it is widely believed that the quantum features of H diffusion are much less pronounced than those in body-centered-cubic metals [1,5,6,9–14] because of their relatively large apparent activation barrier and long jump length. On the other hand, the experimental D values of heavier isotopes of H in fcc Pd, Cu, and Ni are known to exhibit peculiar isotope effects (i.e., reversed isotope dependence and a possible crossover to the normal ordering at a reduced temperature [15–22]), which cannot be explained solely from the difference in the local mode vibrations of the H isotopes at interstitial positions [19]. Because such an effect may arise from a certain competition between different NQEs with different temperature and mass dependencies, theoretical models that properly take into account NQEs are indispensable for identifying the true nature of temperature-dependent ideal H diffusivities.

In our previous work [23], we successfully provided theoretical estimates of D with NQEs for H in Pd by applying *ab initio* modeling based on Feynman's path-integral theory [24] along with density functional theory (DFT). However, the data obtained were limited to a narrow temperature range and available for one isotope of H. In general, the migration of H isotopes proceeds via several different mechanisms, such as (i) coherent tunneling, (ii) thermally activated tunneling, (iii) over-barrier jump, and (iv) fluidlike motion, one of which predominates over the others in a given temperature range [1,10]. In this paper, focusing on regimes (ii) and (iii), we present a consistent and coherent picture of the diffusion kinetics of H isotopes (i.e., protium and tritium) in fcc Pd using a modified approach that treats not only activation barriers, but also preexponential factors to be dependent on temperature and mass, so as to seamlessly capture the onset of quantum tunneling at low temperatures and a transition to the classical limit at high temperatures. Free-energy profiles for H isotope migration with the NQEs were predicted and cast into an Arrhenius diagram of the jump rates and D values of the H isotopes, providing a missing piece of the puzzle for their comprehensive characterization over a wide temperature range.

II. METHODS

A. DFT calculations

The DFT calculations were carried out using the VASP code [25] with the projector-augmented wave (PAW) method

*kimizuka@me.es.osaka-u.ac.jp

[26,27]. The valence electron configurations considered in this study included $1s^1$ for H and $4d^9 5s^1$ for Pd. The exchange-correlation functional was described within the generalized gradient approximation of Perdew, Burke, and Ernzerhof (PBE) [28]. To examine the sensitivity of the exchange-correlation functionals to the energetics of the Pd-H system, the optPBE-vdW [29–31] functional and the hybrid functional of PBE0 [32] were also applied and the results were compared to those obtained from the PBE functional in selected cases (see Appendix A). We considered the $Pd_{32}H_1$ supercell with dimensions of $2a \times 2a \times 2a$ (where a is the lattice constant of the fcc unit cell) under periodic boundary conditions, in which one H atom was initially placed at one of the octahedral (O) or tetrahedral (T) interstitial sites in the fcc structure. Calculations were conducted with a plane-wave energy cutoff (E_{cut}) of 300 eV using a $6 \times 6 \times 6$ Monkhorst-Pack $\boldsymbol{k}$-point mesh [33] for integration over the Brillouin zone. The cell parameters and atomic positions were relaxed within the classical DFT regime (i.e., without NQEs) until the residual forces acting on each atom were less than 10 meV/Å using the Methfessel-Paxton smearing method [34] at a width of 0.2 eV. We used the nudged elastic band (NEB) method [35] with nine intermediate images and a constant cell shape to obtain the minimum energy paths (MEPs) and saddle-point (S) sites for H migration between different sites. Calculations with an E_{cut} of 400 eV and $16 \times 16 \times 16$ $\boldsymbol{k}$-point mesh provided similar values, with a maximum error of 0.01 eV (see Appendix A). The MEPs were then used as the centroid intrinsic reaction coordinates along which the NQEs on the H-diffusion process were evaluated via *ab initio* path-integral molecular dynamics (PIMD) calculations [36,37].

B. *Ab initio* PIMD calculations

To investigate the effects of quantum fluctuations and tunneling on the migration barrier of H in the metal, the PIMD method [38] was employed. According to this approach, the partition function of a quantum particle can be expressed as a configurational integral of a classical object. This object can be approximated as a closed ring polymer (or necklace) consisting of discrete monomers (or beads) connected via harmonic springs with equilibrium distances all equal to zero. The spring constant of the ring polymers is $m_I P/(\beta\hbar)^2$, where m_I represents the mass of the Ith quantum particle in the N-particle system ($1 \leqslant I \leqslant N$), P denotes the number of beads in each ring polymer, β is the inverse temperature $(k_{\mathrm{B}}T)^{-1}$, k_{B} is the Boltzmann constant, T is the absolute temperature, and $\hbar$ is the Planck constant.

In the *ab initio* PIMD, a statistical ensemble of bead configurations $\{\boldsymbol{r}_I^{(s)}\}$ ($1 \leqslant I \leqslant N$, $1 \leqslant s \leqslant P$) is generated according to the discrete path-integral expression for the partition function of N quantum nuclei, given as follows:

$$Z(\beta) = \lim_{P\to\infty}\left[\prod_{I=1}^{N}\left(\frac{m_I P}{2\pi\beta\hbar^2}\right)^{\frac{3P}{2}}\int d\boldsymbol{r}_I^{(1)}\cdots\int d\boldsymbol{r}_I^{(P)}\right] \times \exp\left(-\beta V_{\mathrm{eff}}\left[\left\{\boldsymbol{r}_I^{(s)}\right\}\right]\right). \quad (1)$$

Here, $V_{\mathrm{eff}}[\{\boldsymbol{r}_I^{(s)}\}]$ denotes the effective potential, defined as

$$V_{\mathrm{eff}}\left[\left\{\boldsymbol{r}_I^{(s)}\right\}\right] \equiv \sum_{s=1}^{P}\left[\sum_{I=1}^{N}\frac{m_I P}{2\beta^2\hbar^2}\left(\boldsymbol{r}_I^{(s+1)} - \boldsymbol{r}_I^{(s)}\right)^2 + \frac{1}{P}V\left(\boldsymbol{r}_1^{(s)},\ldots,\boldsymbol{r}_N^{(s)}\right)\right] \quad (2)$$

with the cyclic boundary condition: $\boldsymbol{r}_I^{(P+1)} = \boldsymbol{r}_I^{(1)}$. The interaction potential $V(\boldsymbol{r}_1^{(s)},\ldots,\boldsymbol{r}_N^{(s)})$, which acts between beads with the same bead index s, is obtained by calculating the ground-state energy of the electrons based on DFT (within the adiabatic approximation) for N nuclei fixed in the positions of the sth bead configuration.

To uncouple the harmonic bead-bead interaction term, the bead coordinates were transformed to normal-mode coordinates [38,39]. The fictitious masses associated with the normal-mode momenta were selected for efficient sampling by setting all chain frequencies to the same value. In addition, a massive thermostatting scheme was used in PIMD by attaching separate Nosé-Hoover chains [40–42] with lengths of three to all degrees of freedom, in order to ensure ergodic sampling of the phase space. For each temperature condition (60–1500 K), PIMD calculations were performed in the canonical ensemble for 1000 steps with the time increment $\Delta t = 1$ fs. In these calculations, the multiple-time-step method based on the reference system propagator algorithm [43] was employed for time integration. The harmonic forces and physical forces were updated at intervals of $\frac{1}{50}\Delta t$ and Δt, respectively.

C. Quantum transition state theory for H diffusivities in fcc metals

The path-integral-based reaction free energy introduced by Gillan [9] corresponds to the reversible work of moving the center-of-mass positions (i.e., centroids) of the ring polymers along the reaction coordinate [11,23,44–47]. Each of the obtained images along the MEP were assumed to correspond to the centroid configuration $\boldsymbol{r}^{\mathrm{cent}} = \{\boldsymbol{r}_I^{\mathrm{cent}}\}$ ($1 \leqslant I \leqslant N$) of the ring polymers in the N-particle system. The *ab initio* PIMD calculations were performed for each individual centroid configuration for 1000 steps, using 32 and 12 beads for temperatures below and above 150 K, respectively. Forces acting on the nuclei were calculated from DFT using the PAW-PBE approximation with an E_{cut} of 300 eV and a $6 \times 6 \times 6$ $\boldsymbol{k}$-point mesh. The path-integral average of the centroid force $\boldsymbol{f}^{\mathrm{cent}}(\{\boldsymbol{r}_I^{(s)}\})$ was calculated at 11 temperatures from 60 to 1500 K in a statistical ensemble of bead configurations $\{\boldsymbol{r}_I^{(s)}\}$ with fixed centroid positions. The PIMD-based free-energy profiles were obtained by numerically integrating the centroid mean force along the H-migration pathway $\boldsymbol{q}$ connecting states X and Y, i.e.,

$$\Delta F(\boldsymbol{q}_Y, \boldsymbol{q}_X) = -\int_{\boldsymbol{q}_X}^{\boldsymbol{q}_Y} d\boldsymbol{q}\cdot\frac{\left\langle \boldsymbol{f}^{\mathrm{cent}}\left(\left\{\boldsymbol{r}_I^{(s)}\right\}\right)\delta(\boldsymbol{r}^{\mathrm{cent}} - \boldsymbol{q})\right\rangle_{\mathrm{PI}}}{\left\langle\delta(\boldsymbol{r}^{\mathrm{cent}} - \boldsymbol{q})\right\rangle_{\mathrm{PI}}}, \quad (3)$$

where $\boldsymbol{q}_X$ and $\boldsymbol{q}_Y$ represent the centroid configurations in which the H atom is located either at an O, T, or S site (X = O or T; Y = S), and δ is Dirac's delta function. The bracket denotes the ensemble average of the quantity inside.

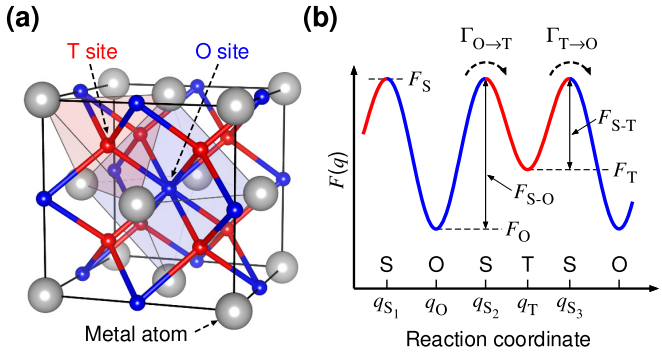

FIG. 1. Schematic illustration of interstitial sites for H atoms in fcc metals. (a) Positions of O and T sites in the fcc lattice. (b) Free-energy profile for successive jumps of a H atom in the O-T network. The S site is the saddle point along the minimum energy path for H migration between neighboring O and T sites.

The differences between the free energies of the system $F_{Y\text{-}X}$ for H at different interstitial sites were calculated as $F_{S\text{-}O} \equiv \Delta F(\boldsymbol{q}_S, \boldsymbol{q}_O)$ and $F_{S\text{-}T} \equiv \Delta F(\boldsymbol{q}_S, \boldsymbol{q}_T)$.

Lattice diffusion of H isotopes in fcc metals occurs by a series of jumps between the O and T interstitial sites such that each O → T jump must be followed by a T → O jump, in which there are two T sites and one O site per metal atom (Fig. 1). Note that the S site is located near the midpoint of each O-T and T-O pathway. The isotropic diffusivity for an O-T network in the fcc lattice without correlation is described as [48]

$$D = \frac{a^2}{2}\rho_O\Gamma_{O\to T} = \frac{a^2}{2}\rho_T\Gamma_{T\to O}, \tag{4}$$

where ρ and Γ denote the equilibrium site probability and jump rate, respectively. The probabilities are written using these two rates as follows:

$$\rho_O = \frac{\Gamma_{T\to O}}{2\Gamma_{O\to T} + \Gamma_{T\to O}}, \quad \rho_T = \frac{\Gamma_{O\to T}}{2\Gamma_{O\to T} + \Gamma_{T\to O}}, \tag{5}$$

which is such that the normalization $\rho_O + 2\rho_T = 1$ holds. In this study, we predicted the jump rates of protium and tritium in fcc Pd using the activation barriers for H isotope migration from the O and T sites (i.e., $F_{S\text{-}O}$ and $F_{S\text{-}T}$, respectively) and the preexponential factor based on the probability distribution in a thermal ensemble derived by Chandler (see, for example, Refs. [49–51]). The jump rate at which the H isotope initially located around the O or T site (q_O or q_T) escapes over the barrier is given as

$$\Gamma_{O\to T} = \frac{v^* \exp(-\beta F_{S\text{-}O})}{\int_{q_{S_1}}^{q_{S_2}} \exp\{-\beta[F(q) - F_O]\}dq},$$
$$\Gamma_{T\to O} = \frac{v^* \exp(-\beta F_{S\text{-}T})}{\int_{q_{S_2}}^{q_{S_3}} \exp\{-\beta[F(q) - F_T]\}dq}, \tag{6}$$

where dq represents a line element along the pathway, i.e., $dq = |d\boldsymbol{q}|$. $F(q)$ denotes the one-dimensional free-energy profile as a function of q between the two tops of the barriers as depicted in Fig. 1. v^* is the forward flux at the barrier top, i.e., $(2\pi\beta m)^{-\frac{1}{2}}$ with m being the mass of the diffusing particle. Note that the model treats both activation barriers and preexponential factors as temperature- and mass-dependent variables accordingly.

III. RESULTS AND DISCUSSION

A. Nuclear quantum effects on H isotope migration

Figure 2 shows the centroid-based free-energy profiles for protium (^{1}H) and tritium (^{3}H) migration between the interstitial sites in Pd over the temperature range of 60–1200 K, obtained from *ab initio* PIMD calculations [36,37]. Note that H isotopes in Pd prefer O sites to T sites. The migration barrier of protium (i.e., $F_{S\text{-}O}$ along the O-T-O pathway) changes drastically as the temperature decreases; it increases in an intermediate-temperature range and then decrease in a low-temperature range. Even in the case of tritium, whose mass is three times larger than that of protium, the migration barrier changes significantly owing to the NQEs: it steadily increases as the temperature decreases down to 75 K. The results indicate that the diffusion of protium and tritium in Pd is impeded by the NQEs over a wide temperature range, which arises from the difference between free volumes (in other words, the difference between curvatures of the potential surface) at the O and T sites [23]. Note that the onset of quantum tunneling is clearly observed at a temperature within the range of 100–150 K and 60–75 K for protium and tritium, respectively. The transition appears to occur fairly suddenly below a certain crossover temperature, which is estimated by [10,52]

$$T_c = \hbar\Omega_b/(2\pi k_B), \tag{7}$$

where $\hbar$ is the Planck constant, and Ω_b is the angular frequency at the barrier top, i.e., the absolute value of the imaginary frequency corresponding to the transition mode. T_c marks the temperature where tunneling and thermally activated barrier crossing are roughly equally important. Based on the analysis of vibrational frequencies, we obtained $\Omega_b = 9.8$ and 5.7 (in $\times 10^{13}$ rad/s) such that $T_c = 119$ and 69 K for protium and tritium, respectively. It is noteworthy that the NQEs are manifested even at relatively high temperatures. Although the free-energy profile approaches its classical limit with increasing temperature, the process of convergence to the limit is quite gradual with temperature, such that the profile does not completely reach the classical limit even at 1200 K. This suggests that the quantum nature of H nuclei is essential for understanding the H-diffusion kinetics in the fcc metal over a wide temperature range.

Quite a few previous studies assumed that the H atom jumps directly between the neighboring O sites [5,6,20] to model the H diffusivity in fcc metals. To examine this possibility, the corresponding free-energy profiles at 60–150 K were calculated using the same computational conditions [Fig. 2(c)]. The direct O-O diffusion barrier is sensitive to temperature and the O-O pathway becomes relatively accessible owing to quantum tunneling as temperature decreases below 150 K. However, it is unlikely that the direct O-O jump mechanism becomes dominant over the O-T-O one in the temperature range above 60 K in light of the fact that the H-migration barrier for the direct O-O pathway is at least

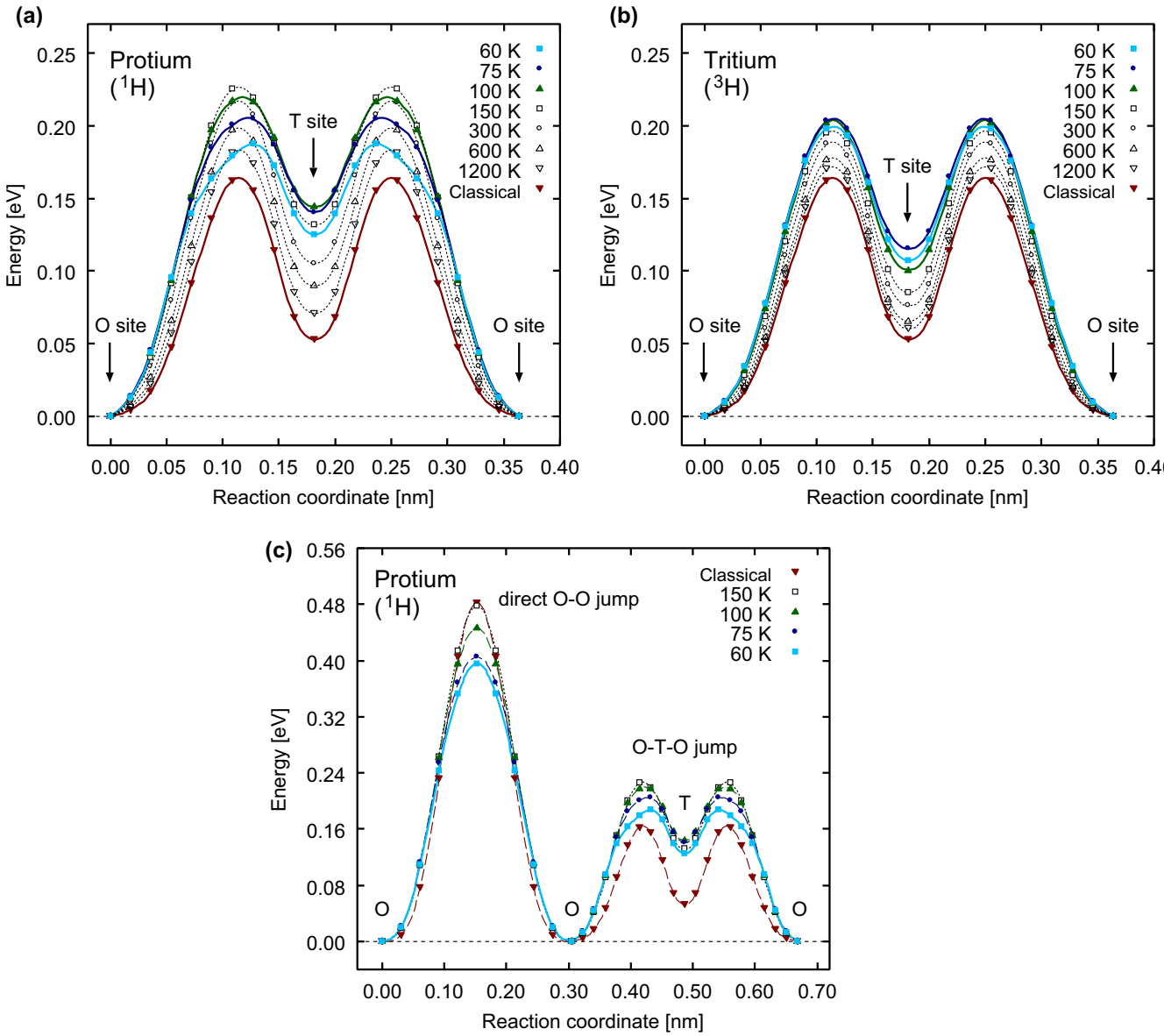

FIG. 2. Free-energy profiles for H isotope migration in Pd at various temperatures. (a) Profiles for protium migration along the O-T-O pathway, (b) profiles for tritium migration along the O-T-O pathway, and (c) profiles (60–150 K) for protium migration along the direct O-O pathway.

twice as high as that for O-T-O pathway. Coherent tunneling via the direct O-O transition is expected to occur at temperature much below 60 K, although this is beyond the scope of this study.

The magnitude of the statistical error in free-energy profiles was estimated by block averaging with a block size of 100 steps for 9 PIMD calculations, while the first 100 steps were discarded as equilibration steps. We confirmed that the standard deviations of the free energies of the system at each configuration along the H-migration pathway were less than 6 meV at temperatures of 60–150 K and even smaller at higher temperatures. Since the value is clearly small compared to differences in activation barriers among H isotopes in Pd measured in experiments [17,19,22], the present approach has sufficient statistical accuracy to identify temperature dependencies of diffusivities of different H isotopes.

B. Quantum distribution of a H isotope

The anisotropic spread of the ring polymer representing a H isotope is characterized by the radius-of-gyration matrix ($\boldsymbol{R}_{\mathrm{g}}$), defined as [10]

$$(\boldsymbol{R}_{\mathrm{g}})^2_{ij} = \frac{1}{P}\left\langle \sum_{s=1}^{P} \left(r_{Ii}^{(s)} - r_{Ii}^{\mathrm{cent}}\right)\left(r_{Ij}^{(s)} - r_{Ij}^{\mathrm{cent}}\right)\right\rangle_{\mathrm{PI}}, \tag{8}$$

where i, j denote Cartesian components (i, $j = 1, 2, 3$) and r_{Ii}^{cent} is the instantaneous centroid of the Ith ring polymer along the ith Cartesian axis. That is,

$$r_{Ii}^{\mathrm{cent}} = \frac{1}{P}\sum_{s=1}^{P} r_{Ii}^{(s)}. \tag{9}$$

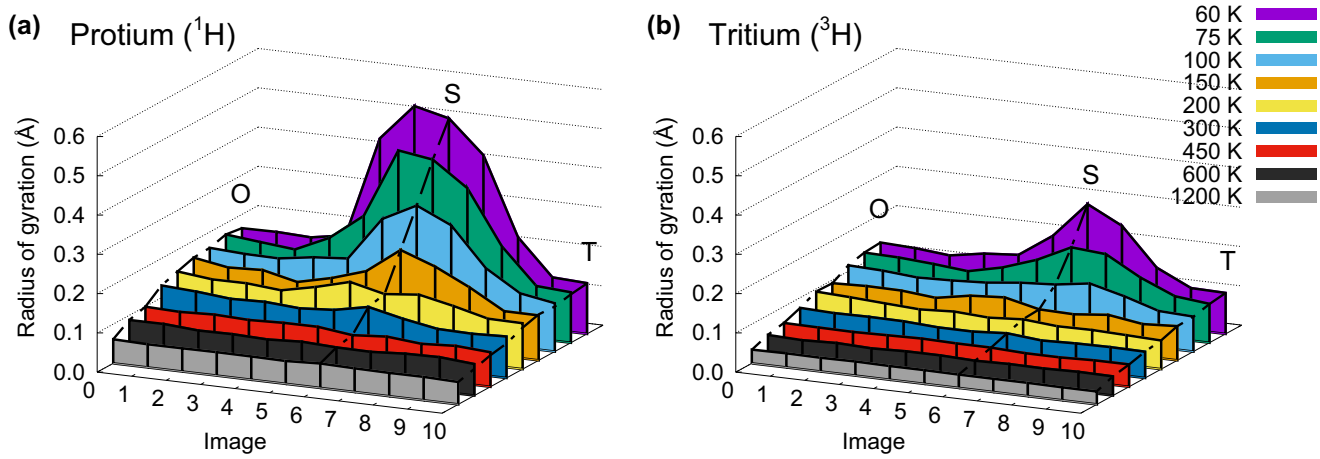

FIG. 3. Largest diagonal element (eigenvalue) of $\boldsymbol{R}_g$ for the quantum distributions of the H-isotope atom along the O-T pathway at various temperatures: results for (a) protium and (b) tritium.

Figure 3 shows the square-root value of the largest eigenvalue of diagonalized $\boldsymbol{R}_g$ of the ring polymer representing a protium and tritium atom along the O-T pathway in Pd at different temperatures. At temperatures above 450 K, the protium- or tritium-atom distribution at all sites is confined and nearly unchanged along the pathway. On the other hand, at temperatures below 200 K, the distribution at the S site broadens substantially and is spread between the O and T sites (parallel to the O-T pathway). Further, the distribution at the site close to the S site also indicates a large spread. These facts suggest that such intersite migrations are significantly influenced by the temperature-dependent quantum delocalization of the H-isotope atom, and that estimating a classical-to-quantum crossover requires not only quantities at the top of the barrier, but also the anharmonicity of each site along the migration pathway.

C. Competition between different NQEs as a key factor influencing unusual temperature dependence

Figure 4 shows the jump rates of the H-isotope atom in fcc Pd as a function of inverse temperature. Notice that $\Gamma_{O\to T}$ and $\Gamma_{T\to O}$ exhibit characteristically different dependence on temperature, viz., an inclined, "reversed S"-shaped curve for $\Gamma_{O\to T}$ and a "C"-shaped curve for $\Gamma_{T\to O}$ on the Arrhenius plot. In the high-temperature region, both rates approach their classical limits, i.e., obtained from Eq. (6) when excluding NQEs, which are represented by almost straight lines in Fig. 4. As temperature decreases, $\Gamma_{O\to T}$ declines in a concave-down fashion and deviates "downward" from the linear behavior in the classical limit. Then, $\Gamma_{O\to T}$ shows an inflection point at approximately T_c and thereafter tends to decrease steadily in a concave-up fashion. Such a trend stems from the *increase, peak, and then decrease* in $F_{S\text{-}O}$ with decreasing temperature owing to NQEs, as seen in Figs. 2(a) and 2(b). It is noteworthy that the results of $\Gamma_{O\to T}$ for protium and tritium are found to be in good agreement with the existing experimental data [20,53] over a wide temperature range. In particular, the gradient of jump rates of H observed [20] is greater in the temperature range around 120–130 K than a low-temperature range (<72 K), which is in line with our calculations.

From the temperature dependence of $\Gamma_{O\to T}$, it is tempting to distinguish three temperature ranges attributable to characteristic diffusion mechanisms: viz., transition from classical (high-temperature) to quantum-fluctuation-dominated (intermediate-temperature) and then to quantum-tunneling-dominated (low-temperature) regimes. Here, we use the term "quantum fluctuation" to mean the motion of quantum particles mainly due to zero-point vibrations and quantization of energy levels among various NQEs. Referring to the high-temperature classical limit of the slope of the Arrhenius plot Q_c, an intermediate-temperature region after going through the former transition has a slope higher than Q_c, indicating the regime in which the H diffusion is inhibited by the elevated barrier due to the quantum fluctuations [23]. After going through the latter transition, a low-temperature region with a slope lower than Q_c is categorized as a quantum tunneling regime.

On the other hand, $\Gamma_{T\to O}$ deviates "upward" from the classical limit and tends to level off at 200–300 K and 100–150 K for protium and tritium, respectively, which is much higher than the estimated T_c. An upturn in the rate indicates the onset of quantum tunneling associated with a transition from the classical to quantum regimes. The temperature dependence of the $\Gamma_{T\to O}$ exhibits a rather familiar, C-shaped curve in the Arrhenius plots. As temperature decreases, the difference between $\Gamma_{O\to T}$ and $\Gamma_{T\to O}$ increases more drastically, as seen in Fig. 4. This indicates that the H isotope diffusion in Pd is dominated by $\Gamma_{O\to T}$ and thus impeded by the NQEs over a wide temperature range.

D. Mechanism of two distinct crossovers in diffusivities of H isotopes

From Eqs. (4) and (5), the diffusion coefficients of H isotopes in fcc Pd were predicted based on the PIMD values of $\Gamma_{O\to T}$ and $\Gamma_{T\to O}$. Figure 5 shows the Arrhenius plots of D for protium and tritium in the temperature range

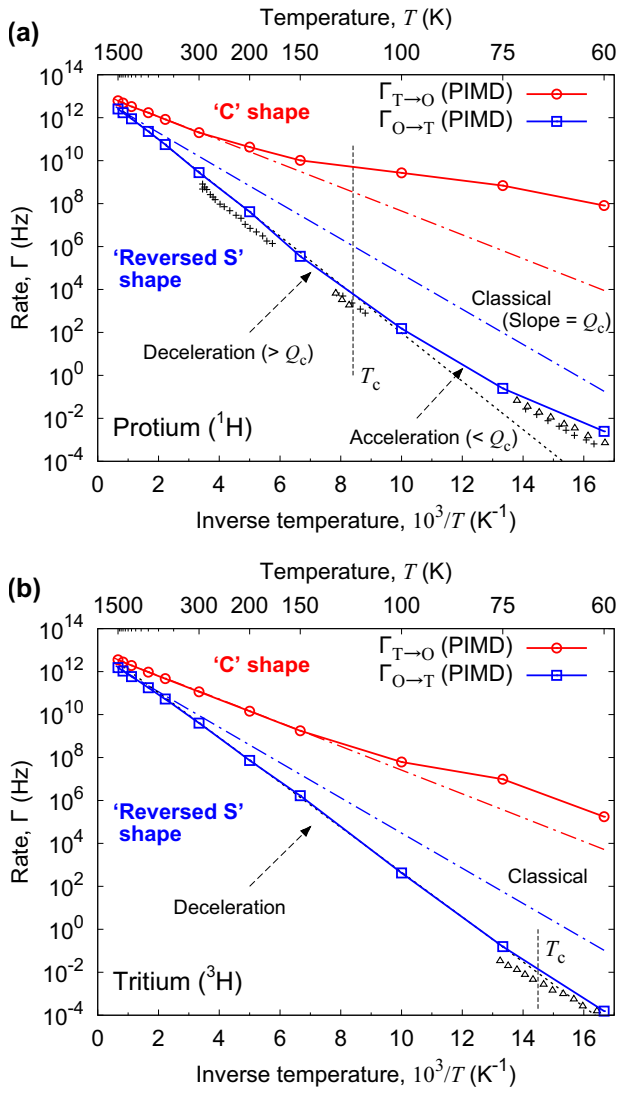

FIG. 4. Arrhenius plots of jump rates of the H-isotope atom in Pd over a temperature range of 60–1500 K: $\Gamma_{O\to T}$ (squares) and $\Gamma_{T\to O}$ (circles) for (a) protium and (b) tritium. The dashed-dotted curves represent the classical limits. The dotted line is an Arrhenius fit of $\Gamma_{O\to T}$ in the intermediate-temperature range of 200–600 K. The experimental data for H and tritium in $Pd_{95}Fe_5$ (triangles) and for H in $PdH_{0.73-0.76}$ (crosses) are taken from Refs. [20] and [53], respectively. Note that the experimental data obtained for H are essentially those for protium. Vertical dotted lines represent the crossover temperatures according to Eq. (7), i.e., $T_c = 119$ and 69 K for protium and tritium, respectively.

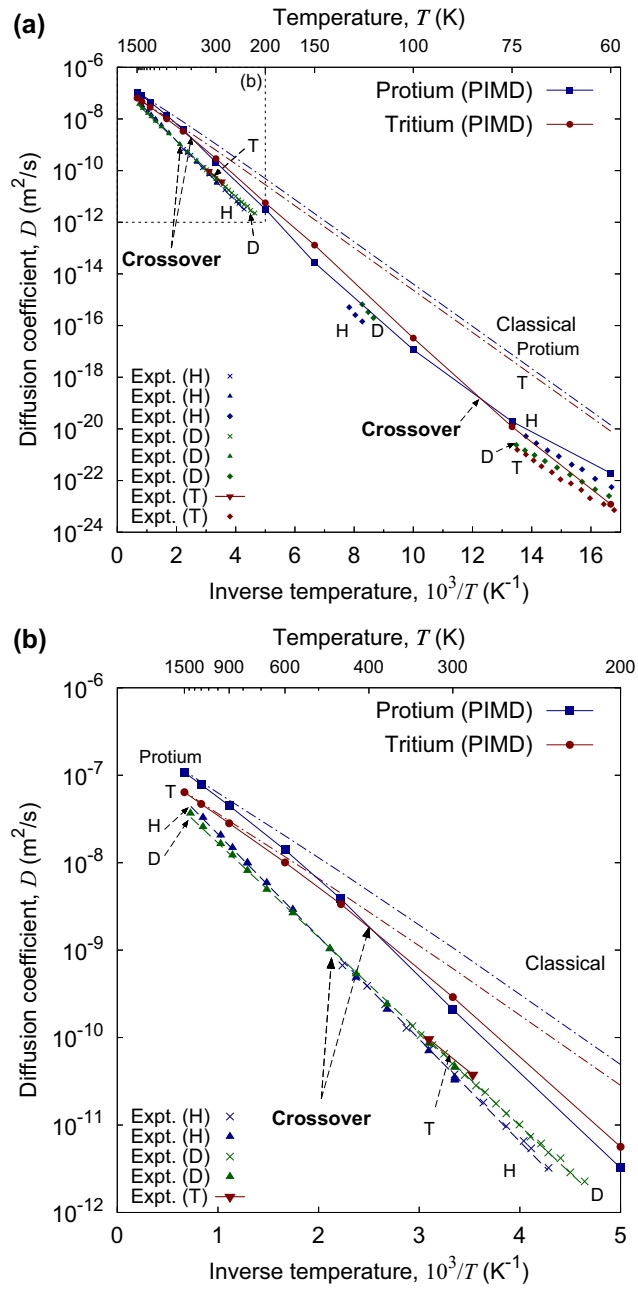

FIG. 5. Diffusion coefficients of H isotopes in Pd in the temperature range of (a) 60–1500 K and (b) 200–1500 K. Solid squares and circles represent the *ab initio* PIMD results for protium and tritium (T), respectively, whose temperature dependence takes a reversed-S shape and thus exhibits the two crossovers at 400 and 80 K. The experimental data for H, deuterium (D), and T are taken from Refs. [17,18,20,22]; triangles (H and D) [22], crosses (H and D) [17], diamonds (H, D, and T) [20], and a line terminated by inverted triangles (T) [18]. Note that the experimental data obtained for H are essentially those for protium.

of 60–1500 K. For comparison, the experimental D values [17,19,20,22] are plotted in Fig. 5. In the PIMD results, the logarithmic D value varies nonlinearly with the inverse temperature, such that the curve is reversed S-shaped because of the characteristic change in $F_{S\text{-}O}$ with respect to temperature. It should be noted that the onset of the deviation from the classical limit was predicted to occur above the upper bound of the temperature range of the experimental data available so far [1,5,6,22]. In the high-temperature region (>1200 K), the classical isotope relations $D_{\text{protium}}/D_{\text{tritium}} = \sqrt{m_{\text{tritium}}/m_{\text{protium}}} = \sqrt{3}$ and $Q_c^{\text{protium}} = Q_c^{\text{tritium}}$ property hold, as seen in Fig. 5(b). As the temperature decreases, D of protium deviates downward from the classical limit and falls below the value of tritium at approximately 400 K. Such behavior is analogous to the crossover of D's between H and deuterium in Pd observed in the experiments at 470 K [17,22] and also supports the experimental observation that

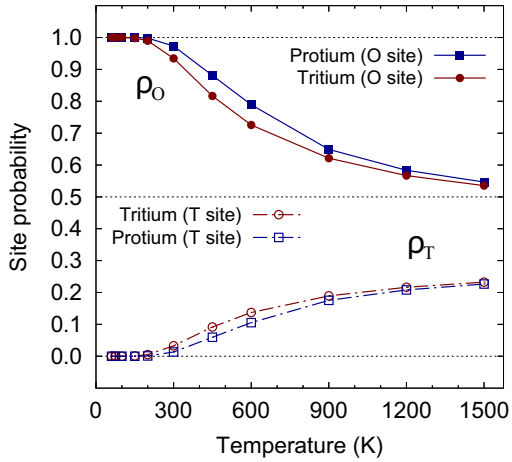

FIG. 6. Temperature dependence of site probabilities for interstitial H isotopes in Pd. From the geometry of the fcc lattice, $\rho_O + 2\rho_T = 1$ holds.

the D values of protium, deuterium, and tritium are in *reverse* order of their masses in the intermediate-temperature region (130–470 K) [17,19,22]. As the temperature decreases further, D of protium crosses over in a concave-up fashion and exceeds that of tritium at approximately 80 K. Note that the D values of H isotopes estimated from the experimental jump rates at low temperatures [20] [from Eq. (4) assuming $\rho_O \approx 1$, which is valid at low temperatures (see Appendix B, Fig. 6)] show a clear downturn in the slope and recover the *normal* ordering below 75 K, which is compatible with our results. Therefore, the *two* crossovers between the normal and reversed isotope effects are attributed to the reversed S-type temperature dependence of the H-isotope diffusivities along the O-T-O pathway.

IV. CONCLUSIONS

Using *ab initio* PIMD, we unveiled the general picture of the temperature-dependent diffusion mechanism of H isotopes in fcc Pd, which has hitherto not been either experimentally or theoretically clarified. Surprisingly, the Arrhenius plot of the jump rate of the H atom from O to T sites had a reversed S-shaped curve, whereas that from T to O sites had a C-shaped curve. The anomalous crossover of isotope effects (i.e., from the normal to reversed and then to normal ordering) on H diffusivity in fcc metals was found to stem from the inherent quantum nature of reversed S-type temperature dependence of D, which accompanies the competition between different NQEs with different temperature and mass dependencies. These results not only call for a revision to the conceptual framework of H diffusion in fcc metals, but also demonstrate a coherent understanding of the quantum behavior of H isotopes.

ACKNOWLEDGMENTS

H.K. would like to thank Y. Fukai for useful discussions. This work was supported by a Grant-in-Aid for Scientific Research (B) (Grant No. 18H01693) from the Japan Society for the Promotion of Science (JSPS) and the Elements Strategy Initiative for Structural Materials (ESISM). M.S. also received support from a Grant-in-Aid for Scientific Research on Innovative Areas (Grant No. 18H05519) from the Ministry of Education, Culture, Sports, Science and Technology (MEXT) of Japan.

APPENDIX A: COMPARISON OF EXCHANGE-CORRELATION FUNCTIONALS

The MEP and the transition state of H migration along the pathway between the neighboring O and T interstitial site were obtained using the NEB method based on DFT for an $Pd_{32}H$ supercell at 3.1 at.% H. The difference between the energies of the system for H in O and T sites is defined as $E_{\text{T-O}}$. Note that a positive $E_{\text{T-O}}$ value indicates that the O site is energetically favorable. Another special site is the saddle-point (S) site located near the midpoint between the O and the T sites. We define the energy of the S site relative to that of the O and T sites as $E_{\text{S-O}}$ and $E_{\text{S-T}}$, respectively.

Table I gives the convergence properties of the classical DFT-NEB calculations with respect to the E_{cut} and $\boldsymbol{k}$-point mesh, using the PBE [28] and optimized PBE van der Waals (optPBE-vdW) functionals [29–31]. We found that a relatively modest E_{cut} (300 eV) and $\boldsymbol{k}$-point mesh ($6 \times 6 \times 6$) produce converged energetic results. For comparison, static single-point calculations using the hybrid functional of PBE0 [32] were performed for the structure optimized with the PBE functional, while isotropically changing the size of the supercell to determine the new energy minimum. As a result, the lattice constant at zero stress (a_0) was reduced by 0.7% compared to that from the PBE functional. The activation barriers obtained from the PBE0 functional were largely compatible with those obtained from the PBE and optPBE-vdW functionals, which indicated that the O-T jump mechanism is dominant for H diffusion in Pd for these functionals. The PBE0 results suggested that the H atom at the T site tends to be relatively stable when a fraction of nonlocal Hartree-Fock exchange is mixed with the DFT exchange-correlation functional. On the other hand, in light of the experimental fact that H and deuterium atoms in bulk Pd prefer O sites to T sites [54,55], the reduction in $E_{\text{T-O}}$ for the PBE0 functional is likely compensated by the NQEs arising from the difference between curvatures of the potential surface at the two sites. For example, in the case of the PBE functional, the difference between the free energies of the system for protium in O and T sites ($F_{\text{T-O}}$) increased by up to 0.09 eV, depending on the temperature owing to the NQEs, as shown in Fig. 2. As a compromise between the accuracy of calculations and computational feasibility, we used the PBE functional with an E_{cut} of 300 eV and a $6 \times 6 \times 6$ $\boldsymbol{k}$-point mesh in this study.

APPENDIX B: SITE PROBABILITY FOR H ISOTOPES

Figure 6 shows the site probabilities for interstitial protium and tritium in Pd as a function of temperature, obtained from Eq. (5). Almost all the H isotopes are located at stable O sites at temperatures below 200 K (i.e., $\rho_O \approx 1$). As temperature increases, a relatively large fraction of H isotopes moves to metastable T sites while maintaining a local thermodynamic equilibrium, which is characterized by the difference between

TABLE I. Convergence tests of classical DFT calculations (without NQEs) for H in Pd. Here, a_0 represents the lattice constant at zero stress, $E_{\text{S-O}}$ (or $E_{\text{S-T}}$) is the energy barrier for H migration from an O (or T) site to a T (or O) site via a saddle-point (S) site, and $E_{\text{T-O}}$ is the difference between the energies of the system for H in O and T interstitial sites. Note that a positive $E_{\text{T-O}}$ value indicates that the O sites are favored.

Functional	E_{cut} (eV)	$\boldsymbol{k}$ points	a_0 (Å)	$E_{\text{S-O}}$ (eV)	$E_{\text{S-T}}$ (eV)	$E_{\text{T-O}}$ (eV)
PBE	300	$6 \times 6 \times 6$	3.942 (O site), 3.947 (T site)	0.16	0.11	0.05
	400	$16 \times 16 \times 16$	3.945 (O site), 3.948 (T site)	0.16	0.11	0.05
optPBE-vdW	300	$6 \times 6 \times 6$	3.939 (O site), 3.942 (T site)	0.12	0.11	0.01
	400	$16 \times 16 \times 16$	3.940 (O site), 3.944 (T site)	0.11	0.11	0.00
PBE0[a]	300	$6 \times 6 \times 6$	3.914 (O site), 3.919 (T site)	0.09	0.13	−0.05

[a]Using the atomic structure optimized with the PBE functional.

the free energies of the system for H isotope in O and T sites. There is a clear tendency that a larger number of tritium atoms than protium atoms tend to remain at T sites. These imply that it is essential to consider both jump rates ($\Gamma_{\text{O}\to\text{T}}$ and $\Gamma_{\text{T}\to\text{O}}$) in the resultant D values of H isotopes, especially at intermediate to high temperatures.

[1] Y. Fukai, *The Metal-Hydrogen System: Basic Bulk Properties*, 2nd ed. (Springer, Berlin, 2005).
[2] J. J. Conde, M. Maroño, and J. M. Sánchez-Hervás, Sep. Purif. Rev. **46**, 152 (2017).
[3] R. Mohtadi and S. Orimo, Nat. Rev. Mater. **2**, 16091 (2016).
[4] R. A. Causey, J. Nucl. Mater. **300**, 91 (2002).
[5] J. Völkl and G. Alefeld, in *Hydrogen in Metals I: Basic Properties*, edited by G. Alefeld and J. Völkl, Topics in Applied Physics Vol. 28 (Springer, Berlin, 1978), pp. 321–348.
[6] H. Wipf, in *Hydrogen in Metals III: Properties and Applications*, edited by H. Wipf, Topics in Applied Physics Vol. 73 (Springer, Berlin, 1997), pp. 51–91.
[7] T. E. Markland and M. Ceriotti, Nat. Rev. Chem. **2**, 0109 (2018).
[8] M. Ceriotti, W. Fang, P. G. Kusalik, R. H. McKenzie, A. Michaelides, M. A. Morales, and T. E. Markland, Chem. Rev. **116**, 7529 (2016).
[9] M. J. Gillan, Phys. Rev. Lett. **58**, 563 (1987).
[10] M. J. Gillan, Philos. Mag. A **58**, 257 (1988).
[11] H. Kimizuka, H. Mori, and S. Ogata, Phys. Rev. B **83**, 094110 (2011).
[12] T. Yoshikawa, T. Takayanagi, H. Kimizuka, and M. Shiga, J. Phys. Chem. C **116**, 23113 (2012).
[13] I. H. Katzarov, D. L. Pashov, and A. T. Paxton, Phys. Rev. B **88**, 054107 (2013).
[14] D. Di Stefano, M. Mrovec, and C. Elsässer, Phys. Rev. B **92**, 224301 (2015).
[15] W. Eichenauer, W. Löser, and H. Witte, Z. Metallkd. **56**, 287 (1965).
[16] L. Katz, M. Guinan, and R. J. Borg, Phys. Rev. B **4**, 330 (1971).
[17] J. Völkl, G. Wollenweber, K.-H. Klatt, and G. Alefeld, Z. Naturforsch. A **26**, 922 (1971).
[18] G. Sicking, M. Glugla, and B. Huber, Ber. Bunsenges. Phys. Chem. **87**, 418 (1983).
[19] G. Sicking, J. Less-Common Met. **101**, 169 (1984).
[20] G. Higelin, H. Kronmüller, and R. Lässer, Phys. Rev. Lett. **53**, 2117 (1984).
[21] K. Yamakawa, K. Nunogaki, and F. E. Fujita, J. Phys. Soc. Jpn. **55**, 877 (1986).
[22] G. L. Powell and J. R. Kirkpatrick, Phys. Rev. B **43**, 6968 (1991).
[23] H. Kimizuka, S. Ogata, and M. Shiga, Phys. Rev. B **97**, 014102 (2018).
[24] R. P. Feynman and A. R. Hibbs, *Quantum Mechanics and Path Integrals* (McGraw-Hill, New York, 1965).
[25] G. Kresse and J. Furthmüller, Phys. Rev. B **54**, 11169 (1996).
[26] P. E. Blöchl, Phys. Rev. B **50**, 17953 (1994).
[27] G. Kresse and D. Joubert, Phys. Rev. B **59**, 1758 (1999).
[28] J. P. Perdew, K. Burke, and M. Ernzerhof, Phys. Rev. Lett. **77**, 3865 (1996).
[29] M. Dion, H. Rydberg, E. Schröder, D. C. Langreth, and B. I. Lundqvist, Phys. Rev. Lett. **92**, 246401 (2004).
[30] G. Román-Pérez and J. M. Soler, Phys. Rev. Lett. **103**, 096102 (2009).
[31] J. Klimeš, D. R. Bowler, and A. Michaelides, J. Phys.: Condens. Matter **22**, 022201 (2010).
[32] C. Adamo and V. Barone, J. Chem. Phys. **110**, 6158 (1999).
[33] H. J. Monkhorst and J. D. Pack, Phys. Rev. B **13**, 5188 (1976).
[34] M. Methfessel and A. T. Paxton, Phys. Rev. B **40**, 3616 (1989).
[35] H. Jónsson, G. Mills, and K. W. Jacobsen, Nudged elastic band method for finding minimum energy paths of transitions, in *Classical and Quantum Dynamics in Condensed Phase Simulations*, edited by B. J. Berne, G. Ciccotti, and D. F. Coker (World Scientific, Singapore, 1998), Chap. 16, pp. 385–404.
[36] D. Marx and M. Parrinello, J. Chem. Phys. **104**, 4077 (1996).
[37] M. Shiga, M. Tachikawa, and S. Miura, J. Chem. Phys. **115**, 9149 (2001).
[38] M. E. Tuckerman, B. J. Berne, G. J. Martyna, and M. L. Klein, J. Chem. Phys. **99**, 2796 (1993).
[39] J. Cao and G. J. Martyna, J. Chem. Phys. **104**, 2028 (1996).
[40] S. Nosé, J. Chem. Phys. **81**, 511 (1984).
[41] W. G. Hoover, Phys. Rev. A **34**, 2499 (1986).
[42] D. J. Tobias, G. J. Martyna, and M. L. Klein, J. Phys. Chem. **97**, 12959 (1993).

[43] G. J. Martyna, M. E. Tuckerman, D. J. Tobias, and M. L. Klein, Mol. Phys. **87**, 1117 (1996).
[44] G. Mills and H. Jónsson, Phys. Rev. Lett. **72**, 1124 (1994).
[45] M. E. Tuckerman and D. Marx, Phys. Rev. Lett. **86**, 4946 (2001).
[46] H. Kimizuka and S. Ogata, Phys. Rev. B **84**, 024116 (2011).
[47] M. Shiga and H. Fujisaki, J. Chem. Phys. **136**, 184103 (2012).
[48] D. R. Trinkle, Philos. Mag. **96**, 2714 (2016).
[49] D. Chandler, J. Chem. Phys. **68**, 2959 (1978).
[50] B. J. Berne, M. Borkovec, and J. E. Straub, J. Phys. Chem. **92**, 3711 (1988).
[51] E. Pollak, J. Chem. Phys. **95**, 533 (1991).
[52] V. I. Goldanskii, Dokl. Akad. Nauk SSSR **124**, 1261 (1959).
[53] R. R. Arons, H. G. Bohn, and H. Lütgemier, Solid State Commun. **14**, 1203 (1974).
[54] J. E. Worsham, Jr., M. K. Wilkinson, and C. G. Shull, J. Phys. Chem. Solids **3**, 303 (1957).
[55] H. Akiba, M. Kofu, H. Kobayashi, H. Kitagawa, K. Ikeda, T. Otomo, and O. Yamamuro, J. Am. Chem. Soc. **138**, 10238 (2016).